Drag Enhancement of Aqueous Electrolyte Solutions in Turbulent Pipe Flow

ARTICLE *in* THE JOURNAL OF PHYSICAL CHEMISTRY B · MARCH 2010

Impact Factor: 3.3 · DOI: 10.1021/jp1005204 · Source: PubMed

3 AUTHORS, INCLUDING:

John Chen
University of Auckland
138 PUBLICATIONS **831** CITATIONS

Drag Enhancement of Aqueous Electrolyte Solutions in Turbulent Pipe Flow

Andrew P. Doherty,*,† Peter L. Spedding,† and John J. J. Chen‡

School of Chemistry and Chemical Engineering, David Keir Building, Queen's University Belfast, Stranmillis Road, Belfast, U.K., BT9 5AG, and Department of Chemical Materials Engineering, University of Auckland, Auckland, New Zealand

Received: January 19, 2010; Revised Manuscript Received: February 16, 2010

Detailed experimental results are presented for both laminar and turbulent flow of aqueous solutions in pipes of different diameters. Nonelectrolytes, such as sugar solutions followed the normal Moody pressure loss curves. Drag enhancement was demonstrated for turbulent flow of aqueous electrolyte solutions but not for laminar flow. The increased pressure drop for turbulent electrolyte flow was attributed to an electroviscous effect and a theory was developed to explain the drag enhancement. The increased pressure drop for the turbulent region of flow was shown to depend on the Debye length in the laminar sublayer on the pipe wall. Reasonable predictions of the increasing drag were obtained for both 1:1 and 2:1 electrolyte solutions.

1. Introduction

Liquid flow in pipes has been shown to follow the Moody diagram,[1] which applies to a wide variety of fluids. One significant deviation has been the drag reduction exhibited by dilute polymer solutions.[2] It has always been assumed that aqueous solutions also follow the Moody diagram. While this has been shown to occur for nonionic aqueous solutions, very little work has been carried out with electrolyte solutions. Gould and Levy[3] and Kratz et al.[4] reported that aqueous calcium chloride solutions obeyed the expected pipe pressure drop within experimental accuracy. However, the flow was only observed up until the late transition region at the start of turbulent flow.

The objective of this work was to examine experimentally and theoretically the pipe frictional pressure drop of aqueous electrolytes particularly under turbulent flow conditions.

2. Experimental Section

The apparatus consisted of three horizontal supported PCV pipes of different diameters and 6.2 m long set one above the other connected between two large vertical headers. The pipe internal diameters were 0.0293, 0.0422, and 0.0524 m determined by measurement and water capacity. Liquid was circulated by a centrifugal pump fed from the base of one header. The pump outlet led to a cooling heat exchanger, a rotameter bank, and a thermometer pocket and into the second header through one of the connecting pipes and then back to the pump inlet. The system was ball-valved and fitted with a pressure relief and bypass system. Pressure tapping points along the top of each horizontal pipe were used to ensure that a constant pressure drop was present over a 4 m length of each pipe for all flows studied. Prior to being introduced to the apparatus, solutions were made up in a weighted tank whereupon the concentrations were checked by density and viscosity measurements. The rotameters were checked by weighed output to confirm the specifications given by the manufacturers. The physical properties of the solutions under test were obtained from International Critical Tables and Handbook of Physics and Chemistry. Manometers with various immiscible liquids were used for pressure drop measurement.

The apparatus was validated using water with the results following the Blasius relation and shown as the lower full line in the figures in the turbulent flow regime above a Reynolds number *Re* of 2300.

The frictional factor ϕ was determined for aqueous solutions of sugar, glycerol, sodium chloride, and sodium carbonate of various concentrations.

3. Experimental Observations

Turbulent water flow data showed that the Blasius relation for smooth pipe flow, given by eq 1

$$\phi = 0.0396Re^{-0.25} \tag{1}$$

was followed up until about $Re < 7 \times 10^{-4}$ where ϕ is the frictional factor. The actual pipe roughness was f/D (f = height of imperfection [m] and D is the pipe diameter [m]), and f was estimated[5] to be 1.56×10^{-5} m. The calculated and experimental uncertainties were within ±1% for water-only flow.

Aqueous sugar and glycerol solutions of various concentrations followed the Hagen−Poiseuille relation for laminar flow up until $Re = 2300$, and the Blasius relation for turbulent flow, up until about $Re \sim 10^5$. The ionic aqueous solutions of NaCl and Na_2CO_3 followed the laminar flow relation. However, both these solutions exhibited an increase in frictional factor, as given by eq 2, where $\bar{\rho}$ is density [km·m^{-3}], u is the velocity [m·s^{-1}], and ΔP is the pressure gradient [kg·m^{-2}·s^{-2}].

$$\phi = \frac{D}{4\bar{\rho}u^2}\Delta P \tag{2}$$

The friction factor was above the Moody diagram values for water in the turbulent flow regime, which is shown as the full line on Figures 1−6. The calculated uncertainty for these data was ±1%, but the experimentally derived uncertainty was ±5%. There was no observed effect with the apparatus in the insulated or earthed condition.

* Corresponding author. E-mail: a.p.doherty@qub.ac.uk.
† Queen's University Belfast.
‡ University of Auckland.

10.1021/jp1005204
Published on Web 03/25/2010

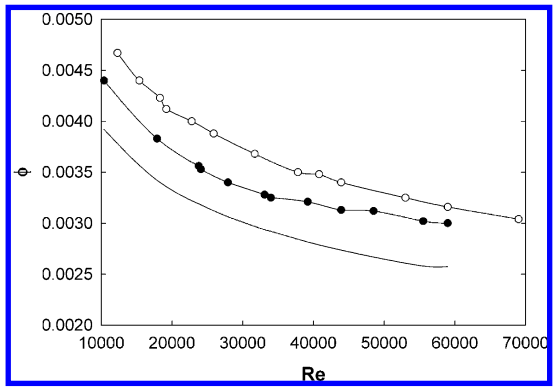

Figure 1. Plot of frictional factor ϕ vs Reynolds number for D = 0.0293 m at NaCl mass fractions of 0.1365 (○) and 0.1037 (●). The solid line is for pure water.

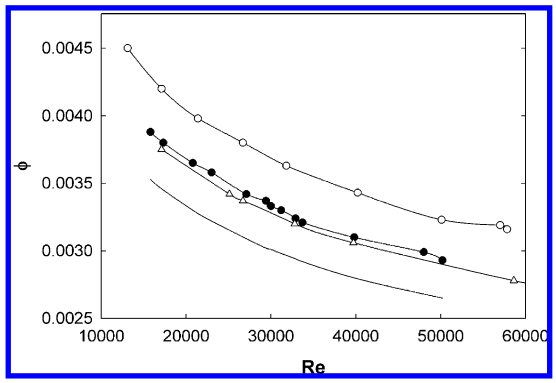

Figure 2. Plot of frictional factor ϕ vs Reynolds number for D = 0.0422 m at NaCl mass fractions of 0.1365 (○), 0.1037 (●), and 0.0894 (Δ). The solid line is for pure water.

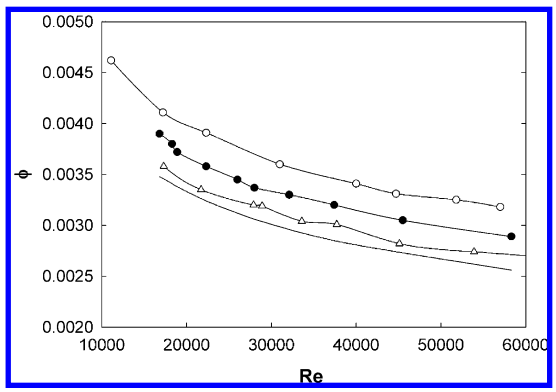

Figure 3. Plot of frictional factor ϕ vs Reynolds number for D = 0.0524 m at NaCl mass fractions of 0.1365 (○), 0.1037 (●), and 0.0894 (Δ). The solid line is for pure water.

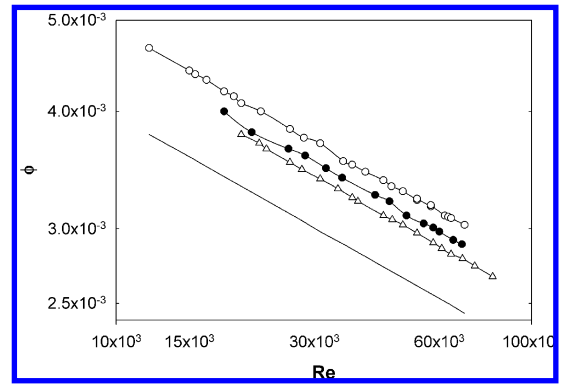

Figure 4. Plot of frictional factor ϕ vs Reynolds number for D = 0.0293 m at Na_2CO_3 mass fractions of 0.0710 (○), 0.0505 (●), and 0.0320 (Δ). The solid line is for pure water.

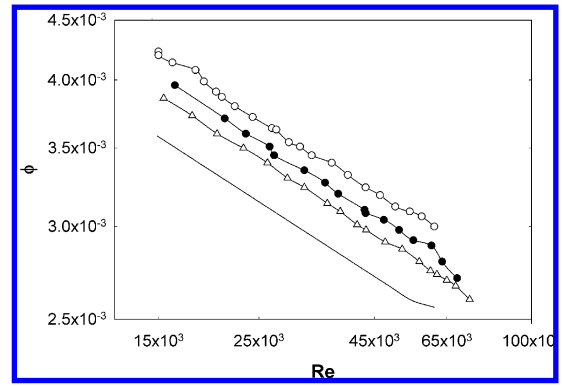

Figure 5. Plot of frictional factor ϕ vs Reynolds number for D = 0.0422 m at Na_2CO_3 mass fractions of 0.0710 (○), 0.0505 (●), and 0.0320 (Δ). The solid line is for pure water.

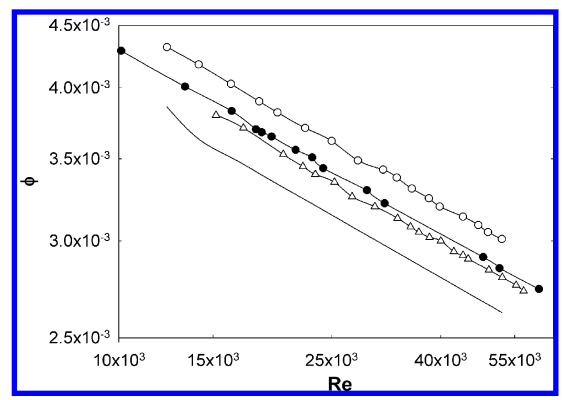

Figure 6. Plot of frictional factor ϕ vs Reynolds number for D = 0.0524 m at Na_2CO_3 mass fractions of 0.0710 (○), 0.0505 (●), and 0.0320 (Δ). The solid line is for pure water.

The observed enhancement of drag in the aqueous electrolyte solutions will now be explored.

3. Theoretical Interpretation of Observations

3.1. Electroviscous Effect. The electroviscous effect was shown by Smoluchowski[6] to increase the viscosity of solid particles suspensions in electrolyte solution over that of the base electrolyte. Kortum[7] showed that with solid surfaces the electroviscous effect was the reverse of electroosmosis when a flowing electrolyte solution established a potential difference or streaming potential.

Conway and Dobry-Duclanx[8] have identified three different electroviscous effects. The primary effect caused by the shear field disturbing the electrical double layer (EDL) surrounding the solid. The secondary effect caused by the overlap of EDLs of neighboring particles. The tertiary effect caused by changes in size and shape of the particle due to the shear field. Only the primary effect is of interest in this work. It has been the subject of much study for suspended particles[9−20] and has been shown to depend on

(a) the size of the Debye length [m] (defined as λ here) of the EDL relative to the size of the suspended particle,

(b) the potential at the slipping plane between the solid and the bulk fluid,

(c) the Peclet number, i.e., diffusive to hydrodynamic forces,

(d) the Hartmann number, i.e., electrical to hydrodynamic forces, and

(e) variation in the Stern layer immediately on the solid surface

Attention has been given to the electroviscous effect for laminar flow in porous solids,[21] capillary tubes,[22−26] and microchannels.[27,28] All these studies provide insight but require some extension to the situation of interest in this work, i.e., turbulent flow of electrolytes in pipes.

3.2. Derivation of the Electroviscous Relationship under Turbulent Flow. A relationship will be developed giving the apparent increased in viscosity η_a [kg·m^{-1}·s^{-1}] of an electrolyte solution in turbulent flow due to the resistance to shear by the EDL on the solid wall attracting ions in the passing liquid. The viscosity increase occurs in the laminar layer on the immediate wall surface, and the geometry can be approximated to a flat plate of unit width (and length) equal to the tube circumference. This is because the actual layer thickness influencing the electroviscosity effect is small compared to the geometry of the overall system. It is necessary to calculate the potential at any point in the fluid as a function of distance x [m] from the plate. The apparent viscosity relation is then obtained by a balance of the forces and the volumetric flow in the laminar layer.

(a) Potential Distribution. At a point x away from a plate, the potential gradient is related to the excess charge density by the Poisson equation, where ψ is the potential [kg·m^2·s^{-3}·A^{-1}], ρ is the charge density [cm^{-3}], and ε is the dielectric constant [C·V^{-1}·m^{-1}].

$$\frac{d^2\psi}{dx^2} = -\frac{\rho_x}{\varepsilon} \tag{3}$$

From the Boltzmann equation for a 1:1 electrolyte (note that for a 1:2 electrolyte, eqs 4 and 7 have the number 3 replacing the number 2),

$$\rho_x = -2n_i e \sinh\left(\frac{e\psi}{kT}\right) \tag{4}$$

where n_i is the ion concentration [m^{-3}], e is the electronic charge [C], k is the Boltzmann constant [kg·m^2·s^{-2}·K^{-1}], and T is the absolute temperature [K]. But

$$\sinh\left(\frac{e\psi}{kT}\right) = \left(\frac{e\psi}{kT}\right) + \frac{1}{6}\left(\frac{e\psi}{kT}\right)^3 + \frac{1}{120}\left(\frac{e\psi}{kT}\right)^5 \tag{5}$$

For small values of $e\psi/kT$only the first term of eq 5 applies. Thus from eqs 3−5

$$\frac{d^2\psi}{dx^2} = \frac{2n_i e^2}{\varepsilon kT}\psi = \frac{\psi}{\lambda^2} \tag{6}$$

where the Debye double layer thickness [m] is

$$\lambda = \left(\frac{\varepsilon kT}{2n_i e^2}\right)^{0.5} \tag{7}$$

Integration of eq 6 remembering that

$$\frac{d^2\psi}{dx^2} = \frac{1}{2}\frac{d}{d\psi}\left(\frac{d\psi}{dx}\right)^2 \tag{8}$$

gives

$$\frac{d\psi}{dx} = \pm\left(\frac{\psi^2}{\lambda^2} + A\right)^{0.5} \tag{9}$$

where A is an integration constant for the positive value of the square root. Since $d\Psi/dx = 0$ at the tube center line and $\psi = 0$ for a thin EDL on the wall, then $A = 0$. Therefore,

$$\frac{d\psi}{dx} = \frac{\psi}{\lambda} \tag{10}$$

Integrating again

$$\frac{x}{\lambda} = \ln\psi + B \tag{11}$$

When $x = 0$, the constant B is

$$B = -\ln\psi_0 \tag{12}$$

Therefore

$$\frac{x}{\lambda} = \ln\left(\frac{\psi}{\psi_0}\right) \tag{13}$$

$$\psi = \psi_0 e^{-x/\lambda} \tag{14}$$

(b) Pressure Force Balance. Consider a unit length laminae parallel to the plate at x of thickness δx. A pressure balance gives

$$\text{viscous retarding force} = \eta\delta x\frac{d^2u}{dx^2} \tag{15}$$

where η is the viscosity [kg·m^{-1}·s^{-1}]

$$\text{pressure force} = \Delta P\delta x \tag{16}$$

$$\text{electrical retarding force} = E\rho_x\,\delta x \tag{17}$$

where E is the streaming potential gradient [V·m^{-1}].

At equilibrium, the liquid moves without acceleration and the pressure gradient is opposed by the retarding forces.

Simplification and a balance gives

$$-\eta\frac{d}{dx}\left(\frac{du}{dx}\right) - E\rho_x = \Delta P \tag{18}$$

From eq 3

$$-\eta\frac{d}{dx}\left(\frac{du}{dx}\right) + \varepsilon E\frac{d}{dx}\left(\frac{d\psi}{dx}\right) = \Delta P \tag{19}$$

Integration gives

$$-\eta\left(\frac{du}{dx}\right) + \varepsilon E\left(\frac{d\psi}{dx}\right) = \Delta P x + A \tag{20}$$

By the Newton law, the wall shear stress R [kg·m^{-1}·s^{-2}] is

$$R = -\eta\frac{du}{dx} \tag{21}$$

Close to the surface in the laminar sublayer, the velocity gradient is linear. Using the concept of the universal velocity profile[5] based on mixing length gives for the laminar layer region

$$\frac{du_x}{dx} = \frac{R}{\eta} = \frac{u_\delta}{\delta} \tag{22}$$

where δ is the laminar sublayer thickness [m].

Substitution in eq 20 gives

$$-R + \varepsilon E\frac{d\psi}{dx} = \Delta P x + A \tag{23}$$

At $x = 0$, $\Psi = \Psi_0$, $u = 0$, and $d\Psi/dx \cong 0$, so the constant $A = -R$ within 10^{-8} %.

Thus integration of eq 20 gives

$$-\eta u + \varepsilon E\psi = -\frac{\Delta P x^2}{2} - Rx + B \tag{24}$$

At $x = 0$, $\Psi = \Psi_0$, $u = 0$ so that the constant B is

$$B = \varepsilon E\psi_0 \tag{25}$$

So eq 24 becomes

$$-\eta u + \varepsilon E(\psi - \psi_0) = \frac{\Delta P x^2}{2} - Rx \tag{26}$$

To handle eq 26, consider flow in the laminar layer between the two flat laminae surfaces of unit width set on the center line at $x = \delta/2$ and distance $2b$ [m], apart as shown in Figure 7.

By a force balance

$$\text{force on AB} = 2bP \tag{27}$$

where P is the pressure [kg·m^{-1}·s^{-2}]

$$\text{force on CD} = -2b\left(P + \left(\frac{dP}{dl}\right)\delta l\right) \tag{28}$$

where l is the length [m]

$$\text{force on surfaces AC and BD} = 2\eta\delta l\left(\frac{du_b}{db}\right) \tag{29}$$

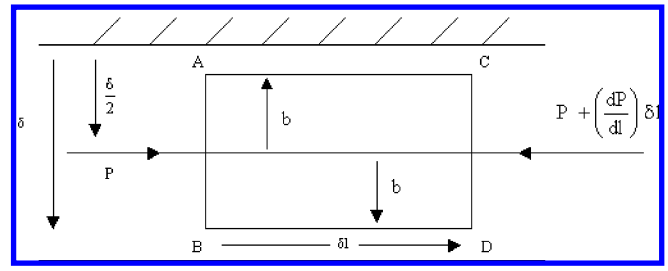

Figure 7. Schematic of laminar layer between two flat laminae plates where δ is the sublayer thickness [m] in the x direction in from the wall, δl is the flowing direction length [m], and P is the pressure [kg·m^{-1}·s^{-2}].

$$2bP - \left(2bP + 2b\left(\frac{dP}{dl}\right)\delta l\right) + 2\eta\delta l\frac{du_b}{db} = 0 \tag{30}$$

$$-b\left(\frac{dP}{dl}\right) + \eta\left(\frac{du_b}{db}\right) = 0 \tag{31}$$

Since $R = \eta\,(du_b/db)$ and $b = \delta/2$

$$R = \Delta P\,\delta/2 \tag{32}$$

So eq 26 becomes

$$-\eta u + \varepsilon E(\psi - \psi_0) = \frac{\Delta P x^2}{2} - \Delta P\frac{x\delta}{2} \tag{33}$$

(c) Apparent Viscosity. The electroviscous effect is best quantified by the determination of the apparent viscosity since it is unclear which pressure drop value should be used for comparison. The following development parallels the general approach adopted by Elton[23] and Li.[28] To obtain a relationship for the apparent viscosity, it is required to determine Q, the liquid volume flowing in the laminar layer in unit time [m^3·s^{-1}]. Taking u from eq 33

$$Q = \int_0^\delta u\,dx = \frac{1}{\eta}\int_0^\delta\left[\frac{\Delta P x}{2}(\delta - x) + \varepsilon E(\psi - \psi_0)\right]dx \tag{34}$$

Substituting eq 14

$$Q = \frac{1}{\eta}\int_0^\delta\left[\frac{\Delta P x}{2}(\delta - x) + \varepsilon E\psi_0(1 - e^{-x/\lambda})\right]dx \tag{35}$$

$$= \frac{1}{\eta}\left[\frac{\Delta P}{2}\left(\frac{\delta x^2}{2} - \frac{x^3}{3}\right) - \varepsilon E\psi_0(x + \lambda e^{-x/\lambda})\right]_0^\delta \tag{36}$$

$$= \frac{1}{\eta}\left[\frac{\Delta P\delta^3}{12} - \varepsilon E\psi_0(\delta + \lambda e^{-\delta/\lambda} - \lambda)\right] \tag{37}$$

The effect of the electrical retardation force of eq 17 will be to increase the viscosity to an apparent value η_a and the pressure force balance will be from eq 18

$$-\eta_a\frac{d}{dx}\left(\frac{du}{dx}\right) = \Delta P \tag{38}$$

TABLE 1: Experimental and Calculated Parameters Associated with NaCl Electrolyte Solutions under Turbulent Flow

parameter	NaCl mass fraction		
	0.0894	0.1037	0.1365
measured from pressure drop viscosity [kg·m^{-1}·s^{-1}]	0.001462 +10% −8%	0.001833 +12% −9%	0.003005 +8% −9%
calculated viscosity [kg·m^{-1}·s^{-1}] eq 41	0.001457	0.001807	0.002926
specific conductance [A·V^{-1}·m^{-1}]	12.710	14. 416	17.834
solution viscosity [kg·m^{-1}·s^{-1}]	0.001161	0.001203	0.001303
dielectric [F·m^{-1}]	695.24×10^{-12}	695.24×10^{-12}	695.24×10^{-12}
surface interface potential [V]	0.00965	0.0135	0.0212
λ [m]	2.30×10^{-10}	2.11×10^{-10}	1.82×10^{-10}

TABLE 2: Experimental and Calculated Parameters Associated with Na_2CO_3 Electrolyte Solutions under Turbulent Flow

parameter	Na_2CO_3 mass fraction		
	0.0320	0.0505	0.0710
measured from pressure drop viscosity [kg·m^{-1}·s^{-1}]	0.001935 ± 12%	0.002189 ± 16%	0.00266 ± 12%
calculated viscosity [kg·m^{-1}·s^{-1}] eq 41	0.001935	0.002187	0.002664
specific conductance [A·V^{-1}·m^{-1}]	3.36	4.72	6.02
solution viscosity [kg·m^{-1}·s^{-1}]	0.001340	0.001344	0.001349
dielectric [F·m^{-1}]	695.24×10^{-12}	695.24×10^{-12}	695.24×10^{-12}
surface interface potential [V]	0.0139	0.0150	0.0177
λ [m]	4.41×10^{-10}	3.48×10^{-10}	2.91×10^{-10}

And following through the development already presented, the integration gives

$$Q = \frac{\Delta P \delta^3}{12\eta_a} \tag{39}$$

Also, from the Helmholtz−Smoluchowski equation[7]

$$E = \frac{\Delta P \varepsilon \zeta}{\eta_a \Omega} \tag{40}$$

where ζ is the wall potential [V] and Ω is the average specific conductivity [A·V^{-1}·m^{-1}].

Substitution of eq 40 into eq 37 gives

$$\eta_a = \eta + \frac{12\varepsilon^2\zeta^2}{\Omega\delta^3}(\delta + \lambda e^{-\delta/\lambda} - \lambda) \tag{41}$$

Figures 1−6 show the experimental friction factors ϕ_{exp} for the ionic solutions to be well above the normal frictional factors ϕ for nonionic liquids as given by eq 1 and shown as full lines in the figures.

Thus, the experimentally derived values give

$$\phi_{exp} = \left(\frac{\Delta P}{u^2}\right)_{exp} \frac{D}{4\bar{\rho}} \tag{42}$$

The frictional factor is independent of viscosity unlike the Reynolds number. Any increase in viscosity to η_a above the International Critical Tables values for η will be found from the coincidence of eqs 1 and 42, thus leading to the apparent viscosity of the electrolyte solution from experimental data.

$$\phi_{exp} = 0.0396\left(\frac{Du\bar{\rho}}{\eta_a}\right)^{-0.25} \tag{43}$$

4. Discussion

Water and nonelectrolyte solutions followed the Moody diagram for both laminar and turbulent flow. Hunter[21] and Elton[23] have reported drag enhancement in capillaries for these types of fluids in laminar flow. Such an effect only took place with diameters well below 10^{-7} m and could not have been observed in this work. Here, drag enhancement was recorded in turbulent pipe flow of ionic aqueous solutions but not in laminar flow in which the normal Hagen−Poiseuille relation was followed and where electroviscous effects will be negligible. The drag enhancement was directly related to concentration. The average experimental and calculated values of apparent viscosity are detailed in Tables 1 and 2. The electroviscous effect occurred only within the confines of the Debye wall layer but its effect on the wall shear stress extended through the whole of the laminar sublayer. The δ/λ relation exhibited an inflection at the value of unity. Therefore, with eq 41 it seemed reasonable to assign a value to δ equal to the Debye length λ. Agreement between theory and experimental was reasonable for the sodium chloride solutions as indicated in Table 1. The sodium carbonate systems gave values of calculated and experimental viscosities detailed in Table 2. Again, these were reasonable predictions of the apparent viscosity.

The actual mechanism invoked was that ions were attached to the pipe wall and attracted those in the bulk of the flowing fluid. The overall effect was to pull back the passing fluid giving an increased viscosity to η_a. The Debye length for the simple sodium chloride electrolytes was of the order of 2×10^{-10} m whereas the ionic diameter and the hydrated ionic diameter were of the order of 3×10^{-12} and 7×10^{-10} m, respectively. It is suggested that the first layer of ions attached to the wall, usually called the Stern layer, was composed of ions while subsequent hydrated ions were beyond the Debye distance. At distances greater than the Debye length ions are beyond the EDL since, at λ, the potential is about $0.05\psi_0$. Consequently, the electroviscous drag enhancement effect was due to the action of the ions within the Stern layer.

The solutions of sodium carbonate exhibited an effect similar to that observed for the sodium chloride case. Hoverer, the sodium carbonate solutions gave a pH range of 11.44−11.49, rising with concentration, indicating that about 7% of the salt was present as the bicarbonate with the rest being the carbonate.

The effect would be to alter, by a few percent, the calculation of the Debye length of eq 7 and the values given in Table 2.

5. Conclusions

The experimental data showed that the flow of aqueous solutions normally followed the Moody diagram of pressure drop against flow rate and surface state. However, aqueous electrolyte solutions were shown to possess drag enhancement qualities for turbulent pipe flow but not in laminar flow. Measurement of viscosity is conducted in the laminar region and not the turbulent region of flow, so any effect in the latter type of flow would not be registered in the viscosity term.

An electroviscous effect was advanced to explain the drag enhancement and an equation derived from consideration of electrolyte solution theory. Agreement between theory and experiment was reasonable for both 1:1 and 2:1 electrolyte solutions. The electrostatic attraction of the adsorbed layer of ions on the pipe inner wall attracted passing ions in the bulk fluid beyond the EDL and provides a mechanism for the observed electroviscous effect.

Further detailed work with other electrolytes and various solution concentrations should enable insight to be obtained on the ionic interactions in the EDL particularly under electrically charged conditions.

References and Notes

(1) Moody, L. F. *Trans. Am. Soc. Mech. Eng.* **1944**, *66*, 671–684.
(2) Sarin, J. G.; Virk, P. S. Drag Reduction. *Am. Inst. Chem. Eng., Symp Ser.* **1977**, *67*, 1–111.
(3) Gould, R. E.; Levy, M. E. Flow of brine in Pipes. *Univ. Illinois Eng. Exp. Stn. Bull.* **1928**, 1–182.
(4) Kratz, A. P.; MacIntire, H. J.; Gould, R. E. Flow of brine in Pipes. *Univ. Illinois Eng. Exp. Stn. Bull.* **1931**, 1–222.
(5) Coulson, J. M.; Richardson, J. F. *Chemical Engineering*, 3rd ed.; Academic Press: New York, 1977; Vol 1, pp 42−43.
(6) Smoluchowski, M. *Kolloid Z.* **1916**, *18*, 190–195.
(7) Kortum, G. *Treatise in Electrochemistry*, 2nd ed.; Elsevier: Amsterdam, 1965; p 428.
(8) Conway, B. E.; Dobry-Duclanx, A. In *Rheology Theory and Applications*; Eirich, F., Ed.; Academic Press: New York, 1960; Vol. 3, p 83.
(9) Booth, F. *Proc. R. Soc.* **1950**, *203A*, 533–551.
(10) Street, N. A. *J. Colloid Sci.* **1958**, *13*, 288–290.
(11) Stone-Masui, J.; Watillon, A. *J. Colloid Interface Sci.* **1968**, *28*, 187–202.
(12) Russel, W. B. *J. Fluid Mech.* **1978**, *85*, 209–232.
(13) Russel, W. B. *J. Fluid. Mech.* **1978**, *85*, 673–683.
(14) Lever, D. A. *J. Fluid Mech.* **1979**, *92*, 421–433.
(15) Sherwood, J. D. *J. Fluid Mech.* **1980**, *101*, 609–629.
(16) Watterson, I. G.; White, L. R. *J. Chem. Soc., Faraday Trans.* **1981**, *77*, 1115–1128.
(17) Hinch, E. J.; Sherwood, J. D. *J. Fluid Mech.* **1983**, *132*, 337–347.
(18) Dukhin, A. S.; Van De Vent, J. G. M. *J. Colloid Interface Sci.* **1993**, *158*, 85–95.
(19) Sherwood, J. D.; Rubio-Hernandez, F. J.; Ruiz-Reina, E. *J. Colloid Interface Sci.* **2000**, *228*, 7–13.
(20) Rubio-Hernandez, F. J.; Ruiz-Reina, E.; Gomez-Merino, A. I.; Sherwood, J. D. *Rheol. Acta* **2001**, *40*, 230–237.
(21) Hunter, R. J. *Zeta Potentials in Colloid Science*; Academic Press: New York, 1981.
(22) Bull, H. B. *Kolloid Z.* **1932**, *60*, 130–132.
(23) Elton, G. A. H. *Proc. R. Soc.* **1948**, *194A*, 259–274.
(24) Elton, G. A. H. *Proc. R. Soc.* **1948**, *194A*, 275–287.
(25) Elton, G. A. H. *Proc. R. Soc.* **1949**, *198A*, 581–589.
(26) Davies, J. J.; Rideal, E. K. *Interfacial Phenomena*, 2nd ed.; Academic Press: New York, 1963.
(27) Masliyah, J. H.; Bhattachaejee, S. *Electrokinetic and Colloid Transport Phenomena*; Wiley: New York, 2006.
(28) Li, D. Q. *Electrokinetics in Microfluidics*; Elsevier: Amsterdam, 2004.

JP1005204